Isotopically Labeled Nanoparticles at Relevant Concentrations: How Low Can We Go? The Case of CdSe/ZnS QDs in Surface Waters

Nurul Supiandi, G. Charron, M. Tharaud, L. Cordier, J.-M. Guigner, M. F Benedetti, Y. Sivry

Isotopically labelled nanoparticles at relevant concentrations: how low can we go? - The case of CdSe/ZnS QDs in surface waters

*Nurul I. Supiandi[†], G. Charron[‡], M. Tharaud[†], L. Cordier[†], J.-M. Guigner[Δ], M. F. Benedetti[†] and Y. Sivry[†]**

† Institut de Physique du Globe de Paris, Sorbonne Paris Cité, Univ. Paris Diderot, UMR 7154, CNRS, F-75005 Paris, France

‡ Laboratoire Matière et Systèmes Complexes (MSC), UMR 7057, Université Paris Diderot, Sorbonne Paris Cité, 75013 Paris, France

Δ Institut de Minéralogie, de Physique des Matériaux et de Cosmochimie (IMPMC), 75005 Paris, France

KEYWORDS: detection limits, nanoparticles, isotopic labelling, quantum dots, aquatic matrices, HR-ICP-MS

ABSTRACT. Analytical barriers impose to work at nanoparticles (NPs) concentration orders of magnitude higher than the expected NPs concentrations in the environment. To overcome these limitations, the use of non-traditional stable isotope tracers incorporated in NPs (spiked-NPs) coupled with HR-ICP-MS has been proposed. The performance and efficiency of this analytical method was assessed in the case of quantum dots (QDs). Multi-isotopically labelled $^{111}Cd^{77}Se/^{68}ZnS$ QDs were synthesized and their dissemination in natural aquatic matrices (river, estuarine and sea waters) was modelled at very low concentrations (from 0.1 to 5000 ppt). The QD limits of quantification (QD-LOQ) in each matrix were calculated according to the isotopic tracer. In ultrapure and simple medium (HNO_3 2%), Zn, Cd and Se originated from the QDs were quantifiable at concentrations of 10, 0.3 and 6 ppt, respectively, which is lower than the conventional HR-ICP-MS LOQs. In aquatic matrices, the QD-LOQs increase 10-, 130-, and 250-fold for Zn, Cd, and Se, respectively, but remain relevant of environmental concentrations (3.4 ppt $\leq$ QD-LOQs $\leq$ 2.5 ppb). These results validate the use of isotopically-labelled ENPs at relevant concentrations in experimental studies related to either their fate, behavior or toxicity in most aquatic matrices.

INTRODUCTION

Engineered nanoparticles (ENPs) are widely used in various consumer products due to their exceptional chemical, optical, magnetic or mechanical properties.[1] To name a few, TiO_2 NPs are used as photocatalyst in water and air treatment,[2] or as whitening agent in paints and in food and food packaging products,[3–5] Ag NPs are added to fabrics for anti-bacterial purpose,[6–12] ZnO NPs act as UV absorbers in sunscreens,[13–15] and CeO_2 NPs are incorporated in catalytic converters in the automotive industry.[16] Quantum dots (QDs), namely fluorescent nanocrystals made of semi-conducting materials, are used in lightning and light display devices for color and brightness enhancement, in solar panels and bio-sensors.[17–22] The use and disposal of these products leads to the release of nanomaterials in wastewater or in the environment (*e.g.* surface waters, soils). Surface waters which are known as one of the major vectors of ENPs dispersion in environment,[23] have inspired numerous publications aiming at determining ENPs fate and behavior in surface waters, in particular through assessing their colloidal and chemical stabilities.[24–30] However, these physico-chemical studies were often conducted at ENPs concentrations that are orders of magnitude higher than the levels expected from their dissemination in aquatic environments. The concentration of ENPs has been shown to affect their dissolution and their aggregation state, thereby potentially impacting their behavior. For instance, the increase in ZnO NPs concentrations decreased their dissolution,[31] whereas their homoaggregation increased with increasing concentrations.[32] Therefore, working at environmentally relevant concentrations is critical when studying the fate and behavior of ENPs in natural systems.

Nevertheless, working at realistic concentrations also means overcoming two common analytical barriers: i) unsuitable instrumental detection limits and ii) the geochemical environmental

53 background, *i.e.* the natural occurrence of some constitutive elements of the ENPs in the
54 environment. Recent development of methods such as single counting ICP-MS (sp-ICP-MS) allow
55 the detection of NPs with limit of detections achieving ppt levels. However, when studying the
56 behavior (e.g. dissolution) of a type of NPs in an environmental medium e.g. river/seawater
57 containing already the same constitutive elements as the NPs, sp-ICP-MS will not be able
58 distinguishing between natural and anthropogenic nanomaterial. Hence, recent studies have
59 proposed the use of non-traditional stable isotopes to overcome these analytical barriers, *i.e.* the
60 use of isotopically modified or "spiked" ENPs which can be quantified by Inductively Coupled
61 Plasma Mass Spectrometry (ICP-MS).[33–37] For instance, this strategy was employed to determine
62 the bio-uptake of TiO_2, Ag, and ZnO NPs in aquatic organisms, using ^{47}Ti, ^{109}Ag, ^{67}Zn tracers,
63 respectively.[33,38,39] Quantitative detection of the ENPs was achieved at concentrations as low as
64 5 ppb, 6 ppt, and 1 ppm for $^{47}TiO_2$, ^{109}Ag, and ^{67}ZnO NPs, respectively, showing the advantages
65 of ENPs isotopic labelling. Although the necessity to work at realistic concentrations has been
66 recently discussed,[37–39] the exposure concentrations generally used in many ENPs fate and behavior
67 studies remain higher than the estimated ones in natural media and, so far, none has tried to
68 accurately determine to which extent the labelling of ENPs with stable isotopes would allow to
69 work at the cutting edge of analytical barriers in ENPs fate and behavior studies.
70 In the present study, we aimed to determine for the first time the analytical limits of the ENP
71 isotopic labelling technique in aquatic matrices (river, estuarine, and seawaters). Quantum dots
72 with a CdSe/ZnS core/shell structure enriched in ^{111}Cd, ^{77}Se, and ^{68}Zn (hereafter called multispiked
73 QDs) were synthesized for the first time in this study. Even though the estimated QDs concentration
74 in aquatic environment is less than 1 ppt,[40,41] their increasing environmental release will

unavoidably follow due to the increasing presence of QDs in consumer products, especially electronic devices (*e.g.* TV set or light bulbs) – therefore, CdSe/ZnS QDs make for a worthy analytical case. As a representative example of core/shell-structured nanomaterials, their reactivity is expected to be more complex than that of homogeneous NPs. These ENPs make for a challenging system on which to gauge the analytical limits of the isotopic labelling strategy. These multispiked QDs were then dispersed at very low and environmentally relevant concentrations (ppt-ppb) into the chosen aquatic matrices. Measurements by HR-ICP-MS and subsequent chemometric processing allowed to accurately determine the limits of quantifications according to the element labelled and to the matrix composition (QD-LOQ). Chemometrics was proven to be an efficient analytical approach *e.g.* during method optimization.[42] This work is expected to provide valuable basis to any future study aiming at using isotopically labelled ENPs to determine their fate, behavior, or toxicity in natural media while working at relevant concentrations.

MATERIALS AND METHODS

Composition of aquatic matrices

The Seine river water was chosen first, as it is highly representative of both a natural carbonate-rich system and a highly anthropized watershed, which is relevant next to the possibility of an accidental release of ENPs. The Seine river water sample was collected behind the University Pierre et Marie Curie (Quai Saint-Bernard, Jardin Tino Rossi, Paris, France, 48.8475° N, 2.3614° E), and filtered through a 0.2 µm cellulose acetate membrane, stored in pre-cleaned, acid-washed polyethylene bottles and divided in three subsamples for: i) major and trace elemental analyses, where the aliquot was acidified with 15 N distilled nitric acid to obtain 2% of nitric acid in the

97 samples, ii) analysis of anions (Cl^-, SO_4^{2-}, NO_3^-), and iii) the determination of isotopic labelling
98 limits experiments. Sampling and analytical procedures were described by Benedetti et al.[43] The
99 chemical composition of the Seine water sample is displayed in Table S1.
100 The second surface water chosen was a synthetic seawater (SW), prepared following the
101 American Society for Testing and Materials (ASTM) International guidelines (Table S2).
102 Dissolved Zn, Cd and Se with natural isotopic abundances were also added to this SW at
103 concentrations provided by Seine Normandie Water Agency.[44]
104 Afterwards, from the precedent Seine river water and SW, three different solutions of estuarine
105 waters were prepared by mixing the Seine river water sample and the SW solution (V/V) by the
106 ratios 75:25 (estuarine water 1), 50:50 (estuarine water 2), and 25:75 (estuarine water 3). All waters
107 were stored at 4°C in pre-cleaned, acid-washed polyethylene bottles.
108
109 ***Synthesis of multi-isotopically labelled CdSe/ZnS quantum dots***
110 All chemical products with natural isotopic composition were purchased from Sigma Aldrich:
111 sulfur (S, 99.9%, powder), oleic acid (OA, technical, 90%), trioctylphosphine (TOP, 90%), 1-
112 octadecene (ODE, 90%), chloroform ($CHCl_3$, 99%), and thioglycolic acid (TGA, 99%). Chemicals
113 with modified isotopic composition were purchased from ISOFLEX USA: cadmium oxide (CdO
114 powder) enriched at 96.00% in ^{111}Cd, zinc oxide (ZnO powder) enriched at 99.16% in ^{68}Zn, and
115 selenium (Se powder) enriched at 99.20% in ^{77}Se.
116 A common route towards CdSe/ZnS nanocrystals consists in nucleating CdSe cores by quickly
117 injecting a chalcogenide mixture into a hot organic solution of the metal salts in a process known
118 as the hot injection method. The growth of the ZnS shell is either achieved in a subsequent step or

one-pot in the same step as nucleation, as described by Bae *et al*.[45] In this protocol, cadmium oxide, zinc acetate, elemental selenium and elemental sulfur were used as the metal and chalcogen precursors, respectively. Transposing this route to multi-spiked CdSe/ZnS QDs raised difficulties regarding the availability of isotopically-modified precursors of suitable isotopic enrichments. ^{111}CdO and ^{77}Se powders were commercially available with ^{111}Cd and ^{77}Se abundances markedly different from the natural ones (96.00% and 99.20%, respectively) that could impart a high isotopic contrast to the QDs compared to the natural background. However, zinc acetate was commercially available with a 48% ^{68}Zn abundancy only, which did not contrast enough with the 18% natural abundancy to support detection of the spiked QDs in the ppt range in natural matrices. Therefore, Bae's protocol was adapted to start from ZnO as the zinc precursor, as it was commercially available with 99.16% enrichment in ^{68}Zn.

Multi-spiked CdSe/ZnS QDs were synthesized by the hot injection method in octadecene following an adaptation of the protocol from Bae *et al.*[45] The modification consisted in substituting ^{68}Zn-enriched ZnO for the initial zinc acetate precursor which was not available with a suitable modified isotopic composition.[45] Briefly, 51.364 g (0.4 mmol) of ^{111}Cd-enriched CdO, 325.56 g (4 mmol) of ^{68}Zn-enriched ZnO, 6.746 g (23.88 mmol) of oleic acid, 20 mg (0.2 mmol) of succinic anhydride and 23 mL octadecene were placed in a 100 mL three-necked round bottom flask equipped with a temperature probe, a coil condenser and connected to an inert lane. The flask was nested into a heating mantel whose power was controlled by a temperature controller connected to the temperature probe. The mixture was degassed under 10 mbar, heated to 150°C and maintained under these conditions for 20 min. Next, the montage was filled with N_2 and further heated to 180°C for 10 min and then 250°C for 10 more minutes to fully dissolve the ZnO powder. The

temperature was then increased to 310°C. At this temperature, a mixture of 31.584 mg (0.4 mmol) of ^{77}Se-enriched selenium and 128.28 mg (4 mmol) sulfur dissolved in 3 mL of trioctylphosphine under N_2 atmosphere was quickly injected into the reaction flask under vigorous stirring. Immediately after injection, the temperature was lowered to 300°C and the flask was kept at this temperature for 15 min to promote the growth of the nanocrystals. The flask was then cooled down to room temperature. The QDs were precipitated with 100 mL of acetone by centrifugation at 6000 rpm and then purified to remove excess reactants by redispersion-precipitation cycles twice with 90 mL acetone and once with 40 mL methanol.

Then, water-soluble QDs were prepared by replacing the oleic acid ligands attached to the surface of the QDs with thioglycolic acid (TGA). In a 100-mL round bottom flask, a solution of 10 mL of chloroform and 1.6 mL of thioglycolic acid (TGA) was prepared. Next, the flask was nested into an ultrasonic bath and 460 µL of the multi-spiked QDs stock solution were added under sonication and maintained under sonication for 1 min. The flask was then equipped with a condenser and transferred into a water bath. The reaction mixture was stirred using a stir bar and heated under reflux for 2 hours. After cooling to room temperature, the TGA-coated QDs were precipitated by centrifugation at 6000 rpm and then purified by redispersion-precipitation cycles twice with 10 mL chloroform and once with 10 mL acetone. Finally, the TGA-coated QDs were dispersed in pH 8 borate buffer and purified using Centricon® Centrifugal Filter Units (30kD MWCO) by exchanging the solvent once with a fresh portion of pH 8 borate buffer and 4 times with ultrapure water adjusted at pH 10. The final solution had a volume of 10 mL.

Quantum dots characterization

Optical characterization of QDs was carried out by measuring the UV–vis absorption spectra of the TGA-coated QDs stock solution with Thermo Scientific Evolution™ 600 UV–vis spectrometer. The fluorescence signal was collected using the Horiba Scientific FluoroMax®-4 spectrofluorometer.

Diluted suspensions QDs were deposited on copper grid to observe their sizes and shapes by Transmission Electron Microscopy (TEM), using a JEOL 2100F electron microscope operating at 200 kV and equipped with a field emission gun, a high-resolution UHR pole piece and a Gatan GIF 200l imaging filter. To perform chemical analysis, this microscope was coupled with electron-dispersive X-ray spectroscopy (EDXS) using a JEOL detector with an ultrathin window allowing detection of low atomic mass elements. TEM pictures were analysed with the software ImageJ 1.51n.

The total concentrations of Cd, Se, and Zn in the TGA-coated QDs stock solution were measured by ICP-OES (Thermo Scientific iCAP 6000 Series) after a complete acid digestion with HF/HNO_3 (see protocol in SI) and then after simple acidification (2% of nitric acid) to evaluate the necessity of using complete acid digestion for all experimental samples.

Model dissemination of QDs in aquatic matrices

All materials used in these experiments (PP tubes, bottles and pipette tips) were washed with HCl 1 N to eliminate possible contaminations in trace metals, especially Zn, Cd and Se.

TGA-coated CdSe/ZnS quantum dots were added separately in all 5 selected natural surface waters, at target concentrations varying from 0.1 to 5000 ppt of Zn issued from the QDs, resulting

184 in 0.03 to 1500 ppt in Cd and 0.02 to 1000 ppt in Se. These choices are in the lowest relevant range
185 of the ENPs estimated concentrations in surface waters (ppt to ppb levels).[40] The QDs were also
186 added, with the same target concentrations, in both HNO_3 2% and $NaNO_3$ 0.01M, used as control
187 media, since there is no occurrence of natural Zn, Cd and Se in both solutions, and the
188 $NaNO_3$ 0.01 M solution is representative of the highest typical ionic strength found in river and
189 estuarine waters.[46] All samples were triplicated to assess the experimental reproducibility.
190 After QDs addition to these media, all samples were agitated then acidified to obtain 2% of nitric
191 acid in the samples, then left overnight prior to dilution and analysis. Simple acidification was
192 sufficient to completely dissolve the QDs, thus the complete acid digestion with HF/HNO_3 was not
193 further performed. The acidification step is representative of the final step used in many studies
194 prior to ENPs analysis.[26,27] For HNO_3 2%, $NaNO_3$ 0.01M matrices and Seine river water sample,
195 no further dilution was needed prior the HR-ICP-MS analysis. For synthetic seawater and estuarine
196 water samples, 50-fold dilutions were performed for best instrument performance and stability.[47]
197
198 ***Quantitative analysis by ICP-MS***
199 External standard solutions containing 1, 5, 10, 100, 500, 1000 and 5000 ppt of total Cd, Se and
200 Zn were prepared in HNO_3 2 %. During the whole analysis, a solution containing 5 ppb of rhodium
201 (^{103}Rh) prepared in HNO_3 2% was used as internal standard solution to correct from instrumental
202 drift and mass bias, and connected online to the sample tubing using a T-adaptor. The isotopes of
203 Cd (^{106}Cd, ^{108}Cd, ^{110}Cd, ^{111}Cd, ^{112}Cd, ^{113}Cd, ^{114}Cd and ^{116}Cd), Zn (^{64}Zn, ^{66}Zn, ^{67}Zn, ^{68}Zn and ^{70}Zn),
204 and Se (^{74}Se, ^{76}Se, ^{77}Se, ^{78}Se, ^{80}Se, ^{82}Se) were analyzed with HR-ICP-MS (ThermoScientific
205 Element II). The isotopes ^{105}Pd, ^{115}In, ^{118}Sn, ^{60}Ni and ^{72}Ge were also analyzed to correct possible

206 isobaric interferences.[48] Each intensity used for data treatment corresponds to the average of 15
207 blocks of 3 replicate measurements, allowing an internal reproducibility with standard error better
208 than 5%. Within each session, reproducibility of the multi-element reference material (TM-23.4
209 Lake Ontario water from National Research Council Canada) was checked at the beginning and
210 the end of each analysis sequence and yielded on average 6.6% shift from the certified values. Most
211 of the sub-procedural variation was found to be within the methods stated overall external
212 reproducibility[49] determined on the three experimental replicates.
213
214 ***Calculation of spiked QDs concentrations***
215 The contrast in isotopic compositions between the multi-spiked QDs and the natural background
216 forms the basis of the quantification of the QDs from HR-ICP-MS measurements. The calculation
217 is an adaptation from Dybowska *et al*.[33] and is detailed in SI.
218
219 **RESULTS AND DISCUSSION**
220 ***QDs synthesis and characterization***
221 Prior to the synthesis of multi-spiked QDs, the synthesis protocol was first conducted as a test
222 run using non-isotopically enriched precursors. Green QDs with an emission centered at 540 nm
223 were obtained. Their absorption spectrum features well resolved excitonic peaks and their emission
224 peak has a full width at half maximum (FWHM) of 35 nm, which is in good agreement with the
225 observations of Bae *et al.* (see SI, Figure S1). When the synthesis was conducted with the
226 isotopically enriched precursors, difficulties were encountered regarding the dissolution of the ZnO
227 precursor. To fully dissolve the powder, it was necessary to heat the metal precursor solution up to

250°C and to maintain it at this temperature for 10 minutes. The resulting multi-spiked QDs also have a green emission centered at 540 nm, however the excitonic peaks are damped and the emission linewidth increases to 40 nm (Figure 1a), indicating that the quality of the nanocrystals has degraded slightly compared to that of the test run QDs. Nevertheless, those properties are still comparable to the QDs described in the original report. The QDs size distribution estimated from a TEM image was 7.9 ± 1.1 nm for $n = 250$ (Figure 1b and c). An EDXS spectrum is provided in SI (Figure S2) confirming the presence of Zn, Cd, and Se in the QDs.

To allow QDs dissemination in aqueous matrices, the QDs were functionalized by substituting thioglycolic acid (TGA) with the oleic acid ligands stemming from the initial synthesis. TEM images are provided in SI (Figure S2). The final TGA-coated QDs stock solution in pH 10 water contains 101.1 ± 1.0 ppm of Zn, 31.8 ± 0.3 ppm of Cd, 19.2 ± 0.3 ppm of Se, and 404 ± 41 ppm of S by ICP-OES.

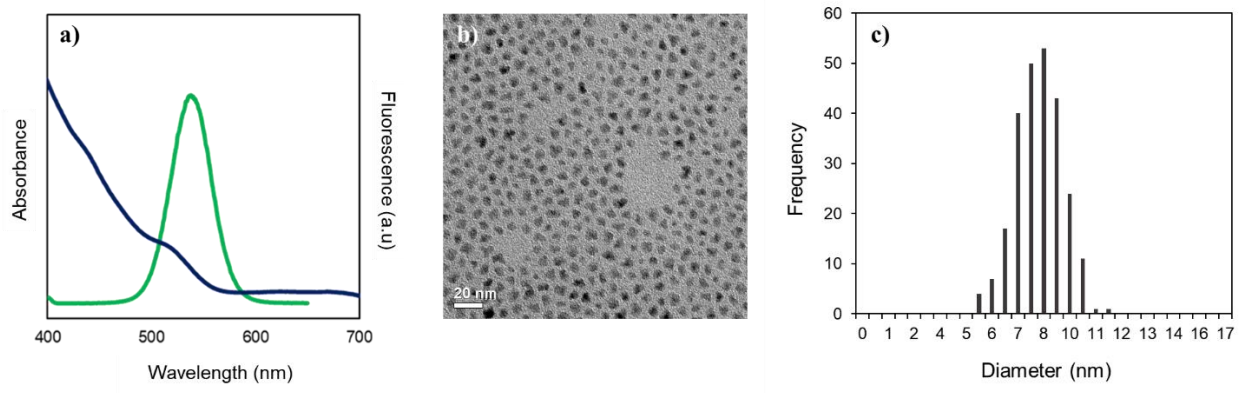

Figure 1. a) UV-vis absorption spectrum (blue line) of the multi-spiked quantum dots and corresponding fluorescence emission spectrum (green line) under 400 nm excitation; b) TEM

244 image of CdSe/ZnS QDs dispersed in chloroform; c) Size distribution of the QDs estimated from
245 the TEM image.

246

247 The isotopic compositions of the multi-spiked QDs regarding Zn, Cd and Se were assessed by
248 HR-ICP-MS and compared to the natural ones (Figure S3). The multi-spiked QDs feature 95.89,
249 99.11 and 98.95% enrichments in ^{111}Cd, ^{68}Zn and ^{77}Se respectively. These abundances are slightly
250 lower than those certified by ISOFLEX for the starting materials, most probably because of minor
251 contamination by chemicals during the synthesis steps. Nevertheless, the QD modified isotopic
252 composition is in sharp contrast with that of the natural background (12.80%, 18.80%, and 7.64%
253 for ^{111}Cd, ^{68}Zn and ^{77}Se respectively).

254

255 ***Assessment of analytical performances***

256 Recovery plots were built by representing the QDs concentration estimated using Eq. S8
257 (hereafter referred to as predicted concentration) as a function of the theoretically known
258 concentrations of QDs added in different matrices (reference concentration in the following), as
259 exemplified in the case of the Seine matrix and on the basis of the ^{68}Zn tracer in Figure 2.

260

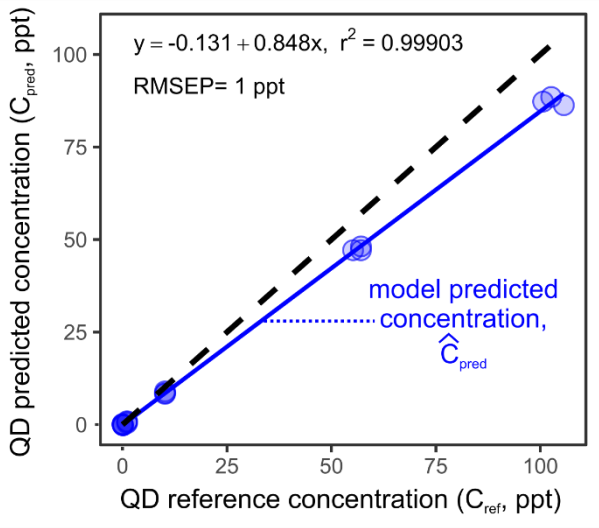

Figure 2. $C_{pred}\ vs.\ C_{ref}$ recovery plots for estimations of QDs concentration based on the ^{68}Zn tracer. The plain blue line indicates the best linear fit and the dashed black line the ideal $C_{pred} = C_{ref}$ recovery plot.

The slope of the best linear regression model leads to the recovery rate of the analytical method, namely the fraction of detected QDs amongst the QDs actually present in the sample (which is related to the bias by $Bias = (1 - Recovery) \times 100$). The precision on the predicted QD concentration was estimated from the Root Mean Square Error of Prediction (RMSEP, defined in Eq. 1) of the regression model. The limit of quantification was chosen as the concentration for which the risk of reporting a false positive or a false negative falls below 0.1%. Briefly, for a set of samples with reference concentration C_0, C_1, C_2, ..., C_n where C_0 corresponds to the "blank" samples, *i.e.* to pure matrix samples, the QD-LOQ was practically determined as follows. A t-test was performed to compare the mean value of the predicted concentrations for the blank samples with that of the predicted concentrations for the samples having the reference concentration C_1. If

276 the t-test concluded that the two means were significantly different at the 99.9% confidence level,
277 then C_1 was designated as the QD-LOQ. If not, then the t-test was conducted using the samples
278 having C_2 concentration. The process was repeated with increasing C_i concentrations until the
279 calculated t value exceeded the critical t-value at the 99.9% confidence level (Figure 3). Since our
280 set of QD spiked samples covers several decades, there are only few experimental points in the
281 vicinity of the QD-LOQ. The QD-LOQ determined from the series of t-test conducted on the
282 experimental data then corresponds to an overestimation of the true QD-LOQ. Therefore, a second
283 series of t-tests were conducted using the experimental blank samples and the model predicted
284 values at intermediate concentrations (with $\widehat{C_{i,pred}}$ as the mean and RMSEP as the standard
285 deviation). This estimation is also conservative since it assigns overestimated standard deviations
286 to points at low reference concentrations as the RMSEP is calculated from data covering several
287 decades. The lowest of the two estimates of QD-LOQ was therefore retained.
288

289 $$RMSEP = \sqrt{\frac{\Sigma\left(C_{pred,i} - \hat{C}_{pred,i}\right)^2}{n}}$$ where n is the number of samples. Eq. 1

290
291

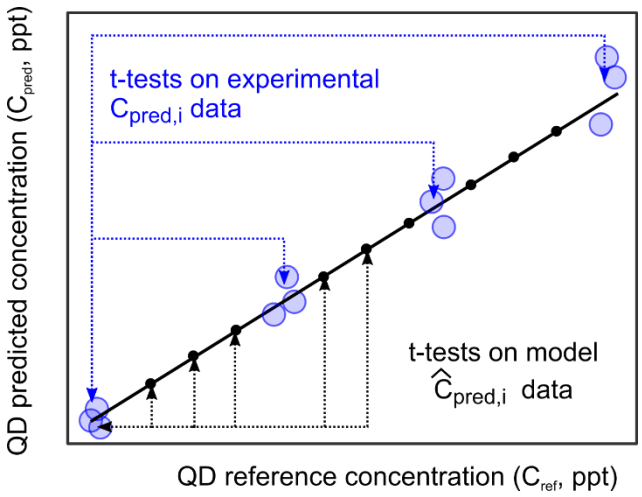

Figure 3. Overview of methodology applied to estimate the QD-LOQ from the recovery plot or its model.

The recovery plots for the ^{68}Zn, ^{111}Cd and ^{77}Se in all investigated matrices are presented in SI (Figures S5 to S24), along with the intensity vs. isotope concentration calibration plots that were used to build them. The biases of all recovery plots are also summarized in SI (Table S3). The *t* values for different QDs concentrations in Cd, Zn and Se calculated in all five matrices are also provided in SI (Table S5 to S7).

Analytical performances: QD-LOQ and precision

Figure 4a displays the observed recovery rates by element. The recovery rates for Cd and Zn are excellent at 99 ± 14 % and 97 ± 13 % on average for all investigated matrices. However, the recovery rate for Se is poor at 19 ± 8 %, indicating that the method lacks sensitivity when the ^{77}Se tracer is used. This is related to the instrumental resolutions at which the three different elements were measured. Briefly, Cd isotopes were measured in low resolution (LR) since this element is

not strongly impacted by polyatomic or isobaric interferences. Zn isotopes had to be measured in middle resolution (MR) to solve polyatomic interference issues (*e.g.* $^{48}Ca^{16}O^{+}$, $^{32}S^{16}O^{18}O^{+}$, $^{40}Ar^{14}N_2^{+}$), resulting in counts numbers about 10% of those typically measured in LR. In the case of Se, it was necessary to perform the measurements in high resolution (HR) to overcome polyatomic interferences mostly caused by argon (Ar), *e.g.* $^{36}Ar^{40}Ar^{1}H^{+}$, $40Ar_2^{+}$, due to the use of Ar as the plasma gas. The intensity signal measured is then around 3% of the total signal measured in LR, which is related to the resolution slit width defining the mass resolution, R (R_{LR} = 300, R_{MR} = 4000, and R_{HR} = 10000). An ANOVA calculation on a model describing the recovery rate as a linear function of the ICP resolution confirmed that the resolution had a significant impact at the 99.9 % confidence level (Tables S9 and S10, model M1). Count numbers were furthered lowered by the fact that the QD concentrations in term of Se were about 2 and 6 times lower on average than that of Cd and Zn respectively. The unsatisfactory results obtained in the case of Se highlight the limits of the spiking method for tracking NPs: for elements subjected to strong polyatomic interferences, it will not be possible to access spike concentrations below the ppb level. However, some specific technical solutions such as hydride generation[50] could allow overcoming this limitation.

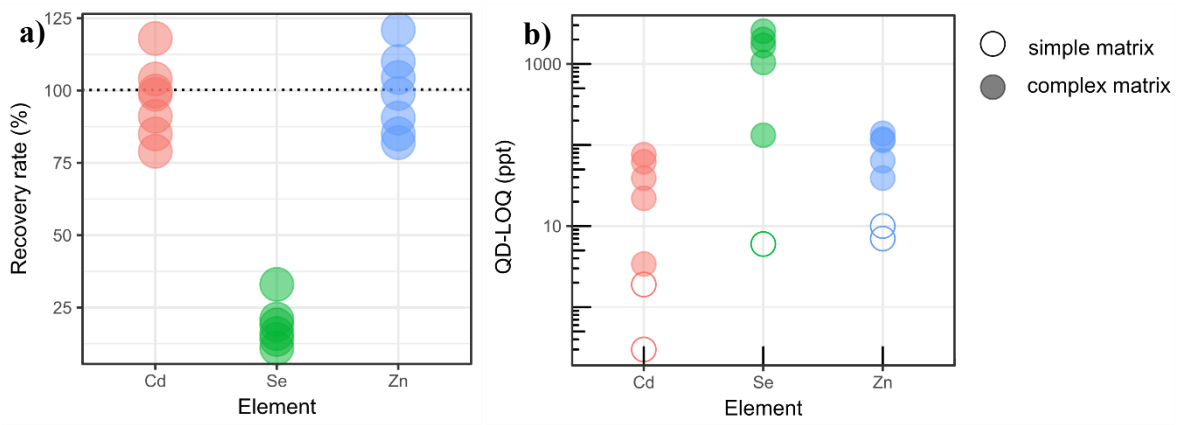

325

326 **Figure 4.** Recovery rates grouped by tracer element, for all matrices confounded (a) and QD-LOQs
327 grouped by tracer element, for simple matrices (empty symbols) and complex matrices (filled
328 symbols) (b).

329

330 Figure 4b and Table 1 display the QD-LOQs of the multi-spiked QDs grouped by tracer element.
331 In oversimplified media (HNO_3 2% and $NaNO_3$ 0.01N) where the background levels in Zn, Cd,
332 and Se are below the HR-ICP-MS LOQ (30, 3, and 62 ppt for Zn, Cd and Se, respectively), the
333 QD-LOQ of Zn, Cd, and Se were 10, 0.3, and 6 ppt, respectively, and in $NaNO_3$ 0.01N were 7 and
334 2 ppt for Zn and Cd, respectively. In contrast, in complex matrices such as Seine river water, the
335 $QD\text{-}LOQ_{Zn}$ increases to 39 ppt. In estuarine water 1 (Seine/SW 75:25), estuarine water 2
336 (Seine/SW 50:50), estuarine water 3 (Seine/SW 25:75), and SW, the $QD\text{-}LOQ_{Zn}$ increases to 139,
337 118, 64, and 112 ppt, respectively. The QD-LOQ in Seine, estuarine water 1, 2, 3, and SW, were
338 3.4, 22, 39, 76, and 62 ppt, respectively for Cd and 132, 1044, 2534, 2003, and 1689 ppt,
339 respectively for Se.

340

Table 1. GBC, QD-LOQ, precision (RMSEP), and RLOQ in different matrices. The conventional HR-ICP-MS LOQ are: Zn 30 ppt, Cd 3 ppt, Se 60 ppt. n.a.: not available.

		HNO_3 2%	$NaNO_3$ 10^{-2} M	Seine	Seine/SW 75:25	Seine/SW 50:50	Seine/SW 25:75	SW
Zn	GBC (ppt)	< LOQ_{Zn}	< LOQ_{Zn}	3718 ± 186	3416 ± 171	2169 ± 108	1493 ± 75	1345 ± 67
	QD-LOQ (ppt)	10	7	39	139	118	64	112
	Precision (ppt)	0.8	1	8	27	42	38	23
	QD-RLOQ	-	-	1.0%	3.9%	5.2%	4.1%	7.7%
Cd	GBC (ppt)	< LOQ_{Cd}	< LOQ_{Cd}	8.4 ± 0.4	23 ± 1.2	42 ± 2.1	81 ± 4.0	75 ± 3.8
	QD-LOQ (ppt)	0.31	1.9	3.4	22	39	76	62
	Precision (ppt)	0.11	0.30	0.78	7.5	8.9	14	10
	QD-RLOQ	-	-	29%	49%	48%	48%	45%
Se	GBC (ppt)	< LOQ_{Se}	n.a.	1069 ± 53	933 ± 47	649 ± 33	617 ± 31	683 ± 34
	QD-LOQ (ppt)	6	n.a.	132	1044	2534	2003	1689
	Precision (ppt)	0.4	n.a.	5	25	64	36	36
	QD-RLOQ	-	-	11%	53%	80%	77%	71%

Unsurprisingly in light of the poor recovery rates observed for Se, QD-LOQ_{Se} are one order of magnitude higher on average than QD-LOQ_{Zn} and QD-LOQ_{Cd}. An ANOVA calculation confirmed that the ICP resolution significantly affects the QD-LOQ at the 99% confidence level (Tables S9 and S11, model M2). In the following, the QD-LOQs according to Se will not be further discussed.

For Cd and Zn tracers, QD-LOQs have mean values of 29 and 70 ppt. However, the QD-LOQs in complex matrices (Seine, sea and estuarine waters) are 37 and 11 times those observed in simple matrices (HNO_3 and $NaNO_3$) for Cd and Zn respectively. Despite this one-order-of-magnitude increase, the multispiked QDs can be detected in realistic surface water samples in concentrations as low as 41 ppt in Cd and 95 ppt in Zn on average, which are about 3 to 6 order of magnitudes lower than the typical concentrations used in ENPs dissemination and toxicity studies (ppb-ppm level).[36,51–53] These results demonstrate the significant added value of the isotopic labelling technique in order to model the environmental fate of ENPs in conditions mimicking as best as possible the natural media.

The increase of the QD-LOQs in complex matrices compared to the ones in simplified media could be explained by three possible arguments. First, simplified media contain virtually zero geochemical background contribution of the spike elements. Indeed, the concentrations in Cd and Zn in the blank samples in the case of HNO_3 and $NaNO_3$ were below the LOQs for their respective isotopes. When moving from these simple media to complex matrices, geochemical background Cd and Zn concentrations increase up to 75 ppt (in sea water) and 3.7 ppb (in Seine water), that is 11 and 3.5 times more than the upper limit of the QD concentration ranges that were investigated in this study. Therefore, the characteristic isotopic fingerprint of the multispiked QDs gets diluted into a large geochemical contribution having the natural isotopic pattern of abundances. This effect will be looked into using the geochemical background concentrations (GBC) of the tracer element in each sample.

Second, complex matrices contain a high concentration of dissolved salts. These can affect intensity readings compared to readings that would have been observed at equal tracer

concentration in HNO_3, which is the matrix in which the $I(^AX)\ vs.\ C_A$ calibration plots were acquired, in a phenomenon known as matrix effect[46] which will be investigated using the ionic strength in the solutions analyzed in the instrument as metric.

Finally, the sea water and estuarine water samples contain high dissolved salt concentrations (Table S2, total dissolved solids TDS_{SW} = 40.8 g/L, I = 0.69M) that may damage the instrument and drastically decrease its sensitivity. These samples had to be diluted prior to ICP-MS analysis, to reach at most the maximum recommended TDS values for ICP-MS analysis (2 g/L)[47,54] resulting in lower tracer concentrations and therefore to lower count numbers. This last effect will be examined using the dilution factor applied to each sample.

On Figure 5, the QD-LOQs according to Cd and Zn tracers were plotted along with the geochemical background concentrations for each matrix and the ionic strength (after dilution if any was required), with an indication of the dilution factor that was applied before ICP-MS analysis. First, the ionic strength of the solutions analyzed in ICP-MS appears constant throughout the various matrices because the acidification at 2% HNO_3 prior to analysis levels it in all analyzed samples. Therefore, matrix effects cannot account for the increase in QD-LOQs observed when moving from simple media to complex aquatic matrices. Second, for both Cd and Zn, the lowest QD-LOQs are the one determined in matrices that did not necessitate dilution prior analysis, so the dilution factor seems to have a significant impact on the QD-LOQ. Last, when Cd is used as a tracer, the QD-LOQs seem to strongly correlate with the GBC. To confirm these graphical findings, ANOVA calculations were conducted. When attempting to model the whole set of QD-LOQs for Cd and Zn, it was found that only the dilution factor and GBC were significant at the 99% confidence level (model M3, Table S12). The QD-LOQs based on Zn were found to depend only

on the dilution factor (model M4, Table S13, Figure S25), while those based on Cd had a strong and exclusive correlation with the GBC (model M5, Table S14, Figure S26). These results are in line with the instrumental constraints pertaining to the Zn and Cd detection. As Zn is analyzed in MR for which signal intensity is on the order of 10% of that of LR measurements, it is expected to be more strongly impacted by further shrinking of the count numbers upon dilution than Cd. On the other hand, the LR measurements in the case of Cd have a smaller discrimination power between isotopes: ^{110}Cd and ^{111}Cd are less distinct in LR than ^{66}Zn and ^{68}Zn in MR, all the more since the latter are separated by two units of mass number. In the presence of increasing GBC of Cd with natural abundance, the ^{111}Cd/^{110}Cd ratio is damped, which may result in impaired estimation of the ^{111}Cd contribution.

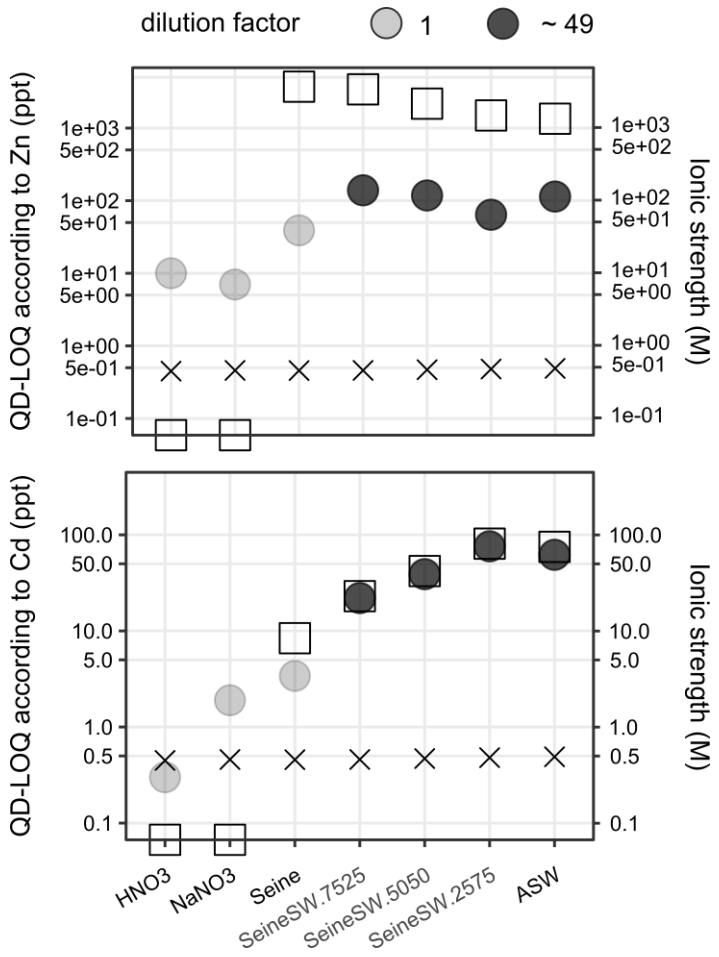

403

404 **Figure 5.** Limits of quantification of multi-spiked QDs (QD-LOQs, dots, in ppt), geochemical
405 background concentration (GBC, squares, also in ppt), ionic strength of the solutions as analyzed
406 in ICP-MS (crosses, in moles.L^{-1}) and dilution factor applied prior to ICP analysis (mapped to the
407 transparency of the dot symbols) in the various aquatic matrices, according to the Zn tracer (top)
408 and to the Cd tracer (bottom).

409

Therefore, the QD-LOQs can be affected by the GBC in the matrices, dilution factor, and analysis resolution. Hence, the relevance of the isotopic spiking method will depend on the element and the matrix targeted in the study. These factors should be considered, for example when choosing the concentration of spiked QDs (or spiked Zn/Cd/Se-containing ENPs) to be used in studies related to ENPs fate and behavior.

To summarize, the limits of quantifications of isotopically labelled CdSe/ZnS quantum dots (QD-LOQs) in natural aquatic matrices were accurately determined by combining HR-ICP-MS and chemometric analysis. QD-LOQs were found varying between 3.4 and 2500 ppt according to the element and the aquatic matrix, which is within the range of ENPs concentrations that are expected in natural surface waters (*e.g.* 2000, 170, and 100, and <10 ppt for TiO_2, ZnO, Ag, and QDs NPs respectively).[23,40,41,55–58] Furthermore, our results indicate that the use of isotopic labelling of ENPs coupled with HR-ICP-MS allows to work at ENPs concentrations about 3 to 6 orders of magnitude lower than the typical concentrations used in numerous ENPs fate and toxicity studies (*e.g.* ZnO at 100 ppb-163 ppm, QDs at 60-3600 ppb).[26,27,29,51–53] Finally, this method does not require the commonly employed feature (*e.g.* optical emission) for fluorescent ENPs such as QDs, which photoluminescent properties can easily be quenched. The QD-LOQs calculated in the present study are up to 2 orders of magnitude more sensitive than methods based on QDs photoluminescence measurement.[59]

Perspective: Relative QD-LOQ

Remarkably, the order of magnitude of relative QD-LOQ (or QD-RLOQ), expressed as the ratio of the QD-LOQ to the sum of QD-LOQ and the total natural element concentration already present

in the matrix (Eq. 2) seems to be characteristic of a given element (Table 1). This variability could then be used to draw estimations of the QD-LOQs in matrices not investigated in the present study, provided that the GBC of that new matrix is known. The knowledge of an expected order of magnitude for the QD-LOQ enables to choose the lowest, and therefore closest to the natural media, concentration of QDs to work with in model dissemination experiments, so as to be able to harvest quantitative data by HR-ICP-MS from said experiments. We recommend though to choose such working QD concentration bearing in mind that due to aggregation phenomena, not all disseminated QDs will actually dissolve.

$$QD\ RLOQ = \frac{QD\ LOQ}{QD\ LOQ+GBC} * 100 \qquad \text{Eq. 2}$$

This percentage allows to accurately assess the efficiency of the spiking method by considering the GBC in the matrix. Globally, we propose that the RLOQ values defined in the present study can be further used to determine the concentration of Zn/Cd/Se-containing ENPs to be used in any experiment related to their fate/behavior/toxicity by using isotopic labelling technique. However, one should consider a slightly higher ENPs concentration when studying their dissolution since the dissolved ENPs concentration is initially unknown. For instance, if Zn from Zn-containing ENPs is expected to dissolve at most 50%, the ENPs concentration used should be at least 2 times the QD-LOQ. Future studies related to ENPs fate, behavior, and toxicity in aquatic environments should be, as much as possible, carried out at environmentally relevant concentrations through the use of isotopically labelled ENPs, on the basis of the QD-LOQs estimated in the present study. The use of relevant concentrations in future experimental work should result in a better and accurate understanding on the ENPs fate, behavior, and toxicity.

ASSOCIATED CONTENT

Supporting Information

Compositions of aquatic matrices (Tables S1 and S2), Acid digestion protocol, Calculations of spiked QDs concentrations for Zn, Cd, and Se, Absorption and emission spectra of the test run QDs (Figure S1), QDs characterization images (Figure S2), Isotopic composition of multispiked QDs (Figure S3), Daily determination of the conventional HR-ICP-MS limit of quantification (LOQ) and its standard error (Figure S4), HR-ICP-MS calibration and spiked QDs concentration recovery plots (Figures S5 to S24), bias of the recovery plots (Table S3), *t* table (Table S4), calculated statistic *t* values (Table S5 to S7), ANOVA test tables (Table S8 to S14) and correlation figures (Figures S25 and S26).

This material is available free of charge via the Internet at http://pubs.acs.org

AUTHOR INFORMATION

Corresponding author

*Email: sivry@ipgp.fr

Author Contributions

The manuscript was written through contributions of all authors. All authors have given approval to the final version of the manuscript. † ‡ Δ These authors contributed equally.

Funding Sources

This research project (nanospike.fr) was fully supported by the French Agency for Food, Environmental and Occupational Health & Safety (ANSES) under the convention N° EST-2013/1/264. Part of this work was supported by the IPGP multidisciplinary program PARI and by Paris-IdF region SESAME Grant n°12015908.

Notes

The authors declare no competing financial interest.

ABBREVIATIONS

ENPs, engineered nanoparticles; FWHM, full width at half maximum; GBC, geochemical background concentrations; QDs, quantum dots, QD-LOQ, limit of quantification of spiked QDs according to the element labelled and to the matrix composition; QD-RLOQ, relative QD-LOQ.

ACKNOWLEDGEMENT

Our thanks go out to the team technical staff, especially to Mr. Mickaël Tharaud and Ms. Laure Cordier, for the assistance during various multi-elemental analyses. Parts of this work were supported by IPGP multidisciplinary program PARI, and by Paris–IdF region SESAME Grant no. 12015908.

490

491 REFERENCES

492 (1) Mitrano, D. M.; Motellier, S.; Clavaguera, S.; Nowack, B. Review of Nanomaterial Aging
493 and Transformations through the Life Cycle of Nano-Enhanced Products. *Environ. Int.* **2015**,
494 *77*, 132–147. https://doi.org/10.1016/j.envint.2015.01.013.
495 (2) Lan, Y.; Lu, Y.; Ren, Z. Mini Review on Photocatalysis of Titanium Dioxide Nanoparticles
496 and Their Solar Applications. *Nano Energy* **2013**, *2* (5), 1031–1045.
497 https://doi.org/10.1016/j.nanoen.2013.04.002.
498 (3) Contado, C. Nanomaterials in Consumer Products: A Challenging Analytical Problem.
499 *Front. Chem.* **2015**, *3*, *48*, 1–20. https://doi.org/10.3389/fchem.2015.00048.
500 (4) Calzolai, L.; Gilliland, D.; Rossi, F. Measuring Nanoparticles Size Distribution in Food and
501 Consumer Products: A Review. *Food Addit. Contam. Part A* **2012**, *29* (8), 1183–1193.
502 https://doi.org/10.1080/19440049.2012.689777.
503 (5) Mattarozzi, M.; Suman, M.; Cascio, C.; Calestani, D.; Weigel, S.; Undas, A.; Peters, R.
504 Analytical Approaches for the Characterization and Quantification of Nanoparticles in Food
505 and Beverages. *Anal. Bioanal. Chem.* **2017**, *409* (1), 63–80. https://doi.org/10.1007/s00216-
506 016-9946-5.
507 (6) Yetisen, A. K.; Qu, H.; Manbachi, A.; Butt, H.; Dokmeci, M. R.; Hinestroza, J. P.;
508 Skorobogatiy, M.; Khademhosseini, A.; Yun, S. H. Nanotechnology in Textiles. *ACS Nano*
509 **2016**, *10* (3), 3042–3068. https://doi.org/10.1021/acsnano.5b08176.
510 (7) Chernousova, S.; Epple, M. Silver as Antibacterial Agent: Ion, Nanoparticle, and Metal.
511 *Angew. Chem. Int. Ed.* **2013**, *52* (6), 1636–1653. https://doi.org/10.1002/anie.201205923.
512 (8) Samsung Electronics. Samsung Silver Nano Technology, Refigerator Silver Nano, Washing
513 Machine Silver Nano, Air Conditioner Silver Nano
514 http://www.samsung.com/my/consumer/learningresources/silvernano/silvernano/ (accessed
515 Sep 2, 2017).
516 (9) Mitrano, D. M.; Ranville, J. F.; Bednar, A.; Kazor, K.; Hering, A. S.; Higgins, C. P. Tracking
517 Dissolution of Silver Nanoparticles at Environmentally Relevant Concentrations in
518 Laboratory, Natural, and Processed Waters Using Single Particle ICP-MS (SpICP-MS).
519 *Environ. Sci. Nano* **2014**, *1* (3), 248–259. https://doi.org/10.1039/C3EN00108C.
520 (10) Kühn, M.; Ivleva, N. P.; Klitzke, S.; Niessner, R.; Baumann, T. Investigation of Coatings of
521 Natural Organic Matter on Silver Nanoparticles under Environmentally Relevant Conditions
522 by Surface-Enhanced Raman Scattering. *Sci. Total Environ.* **2015**, *535*, 122–130.
523 https://doi.org/10.1016/j.scitotenv.2014.12.026.
524 (11) Ibrahim, H. M. M.; Hassan, M. S. Characterization and Antimicrobial Properties of Cotton
525 Fabric Loaded with Green Synthesized Silver Nanoparticles. *Carbohydr. Polym.* **2016**, *151*,
526 841–850. https://doi.org/10.1016/j.carbpol.2016.05.041.
527 (12) Mackevica, A.; Olsson, M. E.; Hansen, S. F. The Release of Silver Nanoparticles from
528 Commercial Toothbrushes. *J. Hazard. Mater.* **2017**, *322*, *Part A*, 270–275.
529 https://doi.org/10.1016/j.jhazmat.2016.03.067.
530 (13) Tyagi, N.; Srivastava, S. K.; Arora, S.; Omar, Y.; Ijaz, Z. M.; AL-Ghadhban, A.; Deshmukh,
531 S. K.; Carter, J. E.; Singh, A. P.; Singh, S. Comparative Analysis of the Relative Potential
532 of Silver, Zinc-Oxide and Titanium-Dioxide Nanoparticles against UVB-Induced DNA

Damage for the Prevention of Skin Carcinogenesis. *Cancer Lett.* **2016**, *383* (1), 53–61. https://doi.org/10.1016/j.canlet.2016.09.026.
(14) Wiechers, J. W.; Musee, N. Engineered Inorganic Nanoparticles and Cosmetics: Facts, Issues, Knowledge Gaps and Challenges. *J. Biomed. Nanotechnol.* **2010**, *6* (5), 408–431. https://doi.org/10.1166/jbn.2010.1143.
(15) Newman, M. D.; Stotland, M.; Ellis, J. I. The Safety of Nanosized Particles in Titanium Dioxide- and Zinc Oxide-Based Sunscreens. *J. Am. Acad. Dermatol.* **2009**, *61* (4), 685–692. https://doi.org/10.1016/j.jaad.2009.02.051.
(16) Senanayake, S. D.; Stacchiola, D.; Rodriguez, J. A. Unique Properties of Ceria Nanoparticles Supported on Metals: Novel Inverse Ceria/Copper Catalysts for CO Oxidation and the Water-Gas Shift Reaction. *Acc. Chem. Res.* **2013**, *46* (8), 1702–1711. https://doi.org/10.1021/ar300231p.
(17) Dai, X.; Deng, Y.; Peng, X.; Jin, Y. Quantum-Dot Light-Emitting Diodes for Large-Area Displays: Towards the Dawn of Commercialization. *Adv. Mater. Deerfield Beach Fla* **2017**, *29* (14). https://doi.org/10.1002/adma.201607022.
(18) Nann, T.; Skinner, W. M. Quantum Dots for Electro-Optic Devices. *ACS Nano* **2011**, *5* (7), 5291–5295. https://doi.org/10.1021/nn2022974.
(19) Pickering, S.; Kshirsagar, A.; Ruzyllo, J.; Xu, J. Patterned Mist Deposition of Tri-Colour CdSe/ZnS Quantum Dot Films toward RGB LED Devices. *Opto-Electron. Rev.* **2012**, *20* (2), 148–152. https://doi.org/10.2478/s11772-012-0019-9.
(20) Shirasaki, Y.; Supran, G. J.; Bawendi, M. G.; Bulović, V. Emergence of Colloidal Quantum-Dot Light-Emitting Technologies. *Nat. Photonics* **2013**, *7* (1), 13–23. https://doi.org/10.1038/nphoton.2012.328.
(21) Kamat, P. V. Quantum Dot Solar Cells. The Next Big Thing in Photovoltaics. *J. Phys. Chem. Lett.* **2013**, *4* (6), 908–918. https://doi.org/10.1021/jz400052e.
(22) Chuang, C.-H. M.; Brown, P. R.; Bulović, V.; Bawendi, M. G. Improved Performance and Stability in Quantum Dot Solar Cells through Band Alignment Engineering. *Nat. Mater.* **2014**, *13* (8), 796–801. https://doi.org/10.1038/nmat3984.
(23) Gottschalk, F.; Sonderer, T.; Scholz, R. W.; Nowack, B. Modeled Environmental Concentrations of Engineered Nanomaterials (TiO2, ZnO, Ag, CNT, Fullerenes) for Different Regions. *Environ. Sci. Technol.* **2009**, *43* (24), 9216–9222. https://doi.org/10.1021/es9015553.
(24) Domingos, R. F.; Tufenkji, N.; Wilkinson, K. J. Aggregation of Titanium Dioxide Nanoparticles: Role of a Fulvic Acid. *Environ. Sci. Technol.* **2009**, *43* (5), 1282–1286. https://doi.org/10.1021/es8023594.
(25) Collin, B.; Auffan, M.; Johnson, A. C.; Kaur, I.; Keller, A. A.; Lazareva, A.; Lead, J. R.; Ma, X.; Merrifield, R. C.; Svendsen, C.; Whitej, J. C..; Unrine, J. M. Environmental Release, Fate and Ecotoxicological Effects of Manufactured Ceria Nanomaterials. *Environ. Sci.: Nano* **2014**, *1* (6), 533–548. https://doi.org/10.1039/C4EN00149D.
(26) Sivry, Y.; Gelabert, A.; Cordier, L.; Ferrari, R.; Lazar, H.; Juillot, F.; Menguy, N.; Benedetti, M. F. Behavior and Fate of Industrial Zinc Oxide Nanoparticles in a Carbonate-Rich River Water. *Chemosphere* **2014**, *95*, 519–526. https://doi.org/10.1016/j.chemosphere.2013.09.110.

(27) Gelabert, A.; Sivry, Y.; Ferrari, R.; Akrout, A.; Cordier, L.; Nowak, S.; Menguy, N.; Benedetti, M. F. Uncoated and Coated ZnO Nanoparticle Life Cycle in Synthetic Seawater. *Environ. Toxicol. Chem.* **2014**, *33* (2), 341–349. https://doi.org/10.1002/etc.2447.
(28) Conway, J. R.; Adeleye, A. S.; Gardea-Torresdey, J.; Keller, A. A. Aggregation, Dissolution, and Transformation of Copper Nanoparticles in Natural Waters. *Environ. Sci. Technol.* **2015**, *49* (5), 2749–2756. https://doi.org/10.1021/es504918q.
(29) Rocha, A. D.; Sivry, Y.; Gelabert, A.; Beji, Z.; Benedetti, M. F.; Menguy, N.; Brayner, R. The Fate of Polyol-Made ZnO and CdS Nanoparticles in Seine River Water (Paris, France). *J. Nanosci. Nanotechnol.* **2015**, *15* (5), 3900–3908. https://doi.org/10.1166/jnn.2015.9276.
(30) Furtado, L. M.; Bundschuh, M.; Metcalfe, C. D. Monitoring the Fate and Transformation of Silver Nanoparticles in Natural Waters. *Bull. Environ. Contam. Toxicol.* **2016**, *97* (4), 449–455. https://doi.org/10.1007/s00128-016-1888-2.
(31) Yung, M. M. N.; Wong, S. W. Y.; Kwok, K. W. H.; Liu, F. Z.; Leung, Y. H.; Chan, W. T.; Li, X. Y.; Djurišić, A. B.; Leung, K. M. Y. Salinity-Dependent Toxicities of Zinc Oxide Nanoparticles to the Marine Diatom Thalassiosira Pseudonana. *Aquat. Toxicol.* **2015**, *165*, 31–40. https://doi.org/10.1016/j.aquatox.2015.05.015.
(32) Keller, A. A.; Wang, H.; Zhou, D.; Lenihan, H. S.; Cherr, G.; Cardinale, B. J.; Miller, R.; Ji, Z. Stability and Aggregation of Metal Oxide Nanoparticles in Natural Aqueous Matrices. *Environ. Sci. Technol.* **2010**, *44* (6), 1962–1967. https://doi.org/10.1021/es902987d.
(33) Dybowska, A. D.; Croteau, M.-N.; Misra, S. K.; Berhanu, D.; Luoma, S. N.; Christian, P.; O'Brien, P.; Valsami-Jones, E. Synthesis of Isotopically Modified ZnO Nanoparticles and Their Potential as Nanotoxicity Tracers. *Environ. Pollut.* **2011**, *159* (1), 266–273. https://doi.org/10.1016/j.envpol.2010.08.032.
(34) Buffet, P.-E.; Amiard-Triquet, C.; Dybowska, A.; Risso-de Faverney, C.; Guibbolini, M.; Valsami-Jones, E.; Mouneyrac, C. Fate of Isotopically Labeled Zinc Oxide Nanoparticles in Sediment and Effects on Two Endobenthic Species, the Clam Scrobicularia Plana and the Ragworm Hediste Diversicolor. *Ecotoxicol. Environ. Saf.* **2012**, *84*, 191–198. https://doi.org/10.1016/j.ecoenv.2012.07.010.
(35) Larner, F.; Dogra, Y.; Dybowska, A.; Fabrega, J.; Stolpe, B.; Bridgestock, L. J.; Goodhead, R.; Weiss, D. J.; Moger, J.; Lead, J. R.; Valsami-Jones, E.; Tyler, C. R.; Galloway, T. S.; Rehkämper, M. Tracing Bioavailability of ZnO Nanoparticles Using Stable Isotope Labeling. *Environ. Sci. Technol.* **2012**, *46* (21), 12137–12145. https://doi.org/10.1021/es302602j.
(36) Khan, F. R.; Laycock, A.; Dybowska, A.; Larner, F.; Smith, B. D.; Rainbow, P. S.; Luoma, S. N.; Rehkaemper, M.; Valsami-Jones, E. Stable Isotope Tracer To Determine Uptake and Efflux Dynamics of ZnO Nano- and Bulk Particles and Dissolved Zn to an Estuarine Snail. *Environ. Sci. Technol.* **2013**, *47* (15), 8532–8539. https://doi.org/10.1021/es4011465.
(37) Laycock, A.; Diez-Ortiz, M.; Larner, F.; Dybowska, A.; Spurgeon, D.; Valsami-Jones, E.; Rehkaemper, M.; Svendsen, C. Earthworm Uptake Routes and Rates of Ionic Zn and ZnO Nanoparticles at Realistic Concentrations, Traced Using Stable Isotope Labeling. *Environ. Sci. Technol.* **2016**, *50* (1), 412–419. https://doi.org/10.1021/acs.est.5b03413.
(38) Bourgeault, A.; Cousin, C.; Geertsen, V.; Cassier-Chauvat, C.; Chauvat, F.; Durupthy, O.; Chanéac, C.; Spalla, O. The Challenge of Studying TiO2 Nanoparticle Bioaccumulation at

Environmental Concentrations: Crucial Use of a Stable Isotope Tracer. *Environ. Sci. Technol.* **2015**, *49* (4), 2451–2459. https://doi.org/10.1021/es504638f.
(39) Croteau, M.-N.; Dybowska, A. D.; Luoma, S. N.; Misra, S. K.; Valsami-Jones, E. Isotopically Modified Silver Nanoparticles to Assess Nanosilver Bioavailability and Toxicity at Environmentally Relevant Exposures. *Environ. Chem.* **2014**, *11* (3), 247–256. https://doi.org/10.1071/EN13141.
(40) Gottschalk, F.; Lassen, C.; Kjoelholt, J.; Christensen, F.; Nowack, B. Modeling Flows and Concentrations of Nine Engineered Nanomaterials in the Danish Environment. *Int. J. Environ. Res. Public. Health* **2015**, *12* (5), 5581–5602. https://doi.org/10.3390/ijerph120505581.
(41) Piccinno, F.; Gottschalk, F.; Seeger, S.; Nowack, B. Industrial Production Quantities and Uses of Ten Engineered Nanomaterials in Europe and the World. *J. Nanoparticle Res.* **2012**, *14* (9), 1–11. https://doi.org/10.1007/s11051-012-1109-9.
(42) Majedi, S. M.; Lee, H. K.; Kelly, B. C. Chemometric Analytical Approach for the Cloud Point Extraction and Inductively Coupled Plasma Mass Spectrometric Determination of Zinc Oxide Nanoparticles in Water Samples. *Anal. Chem.* **2012**, *84* (15), 6546–6552. https://doi.org/10.1021/ac300833t.
(43) Benedetti, M. F.; Dia, A.; Riotte, J.; Chabaux, F.; Gérard, M.; Boulègue, J.; Fritz, B.; Chauvel, C.; Bulourde, M.; Déruelle, B.; Ildefonse, P. Chemical Weathering of Basaltic Lava Flows Undergoing Extreme Climatic Conditions: The Water Geochemistry Record. *Chem. Geol.* **2003**, *201* (1–2), 1–17. https://doi.org/10.1016/S0009-2541(03)00231-6.
(44) Seine Normandie Water Agency. Etude 2008 - Guide toxique (Zn, Cd, Se) http://www.eau-seine-normandie.fr.
(45) Bae, W. K.; Char, K.; Hur, H.; Lee, S. Single-Step Synthesis of Quantum Dots with Chemical Composition Gradients. *Chem. Mater.* **2008**, *20* (2), 531–539. https://doi.org/10.1021/cm070754d.
(46) Garrels, R. M.; Christ, C. L. *Solutions, Minerals, and Equilibria*; Harper & Row, 1965.
(47) McCurdy, E.; Proper, W. Improving ICP-MS Analysis of Samples Containing High Levels of Total Dissolved Solids. *Spectroscopy*. 2014.
(48) Thomas, R. A Beginner's Guide to ICP-MS Part XII — A Review of Interferences. *Spectroscopy* **2002**, *17* (10).
(49) Casadevall, A.; Fang, F. C. Reproducible Science. *Infect. Immun.* **2010**, *78* (12), 4972–4975. https://doi.org/10.1128/IAI.00908-10.
(50) Far, J.; Bérail, S.; Preud'homme, H.; Lobinski, R. Determination of the Selenium Isotopic Compositions in Se-Rich Yeast by Hydride Generation-Inductively Coupled Plasma Multicollector Mass Spectrometry. *J. Anal. At. Spectrom.* **2010**, *25* (11), 1695–1703. https://doi.org/10.1039/C004933F.
(51) Tang, Y.; Li, S.; Lu, Y.; Li, Q.; Yu, S. The Influence of Humic Acid on the Toxicity of Nano-ZnO and Zn2+ to the Anabaena Sp. *Environ. Toxicol.* **2015**, *30* (8), 895–903. https://doi.org/10.1002/tox.21964.
(52) Jackson, B. P.; Bugge, D.; Ranville, J. F.; Chen, C. Y. Bioavailability, Toxicity, and Bioaccumulation of Quantum Dot Nanoparticles to the Amphipod Leptocheirus Plumulosus. *Environ. Sci. Technol.* **2012**, *46* (10), 5550–5556. https://doi.org/10.1021/es202864r.

(53) Xiao, Y.; Ho, K. T.; Burgess, R. M.; Cashman, M. Aggregation, Sedimentation, Dissolution, and Bioavailability of Quantum Dots in Estuarine Systems. *Environ. Sci. Technol.* **2017**, *51* (3), 1357–1363. https://doi.org/10.1021/acs.est.6b04475.
(54) Thermo Fischer. *Thermo Fischer Scientific, Application Note 30003, Determination Trace Elements Clinical Samples High-Resolution-ICP-MS*; 2007.
(55) Gottschalk, F.; Sun, T.; Nowack, B. Environmental Concentrations of Engineered Nanomaterials: Review of Modeling and Analytical Studies. *Environ. Pollut.* **2013**, *181*, 287–300. https://doi.org/10.1016/j.envpol.2013.06.003.
(56) Gottschalk, F.; Ort, C.; Scholz, R. W.; Nowack, B. Engineered Nanomaterials in Rivers – Exposure Scenarios for Switzerland at High Spatial and Temporal Resolution. *Environ. Pollut.* **2011**, *159* (12), 3439–3445. https://doi.org/10.1016/j.envpol.2011.08.023.
(57) Tiede, K.; Hassellöv, M.; Breitbarth, E.; Chaudhry, Q.; Boxall, A. B. A. Considerations for Environmental Fate and Ecotoxicity Testing to Support Environmental Risk Assessments for Engineered Nanoparticles. *J. Chromatogr. A* **2009**, *1216* (3), 503–509. https://doi.org/10.1016/j.chroma.2008.09.008.
(58) Dumont, E.; Johnson, A. C.; Keller, V. D. J.; Williams, R. J. Nano Silver and Nano Zinc-Oxide in Surface Waters – Exposure Estimation for Europe at High Spatial and Temporal Resolution. *Environ. Pollut.* **2015**, *196*, 341–349. https://doi.org/10.1016/j.envpol.2014.10.022.
(59) Xu, S.; Wang, C.; Xu, Q.; Li, R.; Shao, H.; Zhang, H.; Fang, M.; Lei, W.; Cui, Y. What Is a Convincing Photoluminescence Quantum Yield of Fluorescent Nanocrystals. *J. Phys. Chem. C* **2010**, *114* (34), 14319–14326. https://doi.org/10.1021/jp100696e.

686

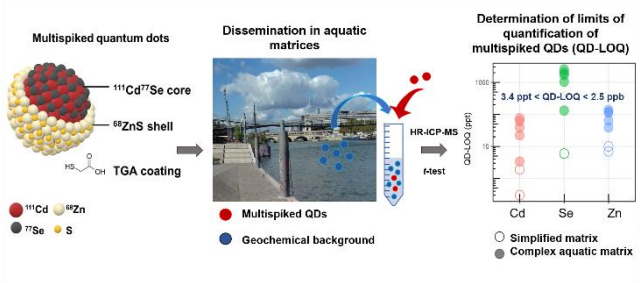

687

688 **For Table of Contents Only**